# An Analysis of CMRR Degradation in Multi-Channel Biosignal Recording Systems

Omid Malekzadeh-Arasteh<sup>®</sup>, *Graduate Student Member, IEEE*, Ahmad Reza Danesh, *Graduate Student Member, IEEE*, An H. Do, Zoran Nenadic<sup>®</sup>, *Senior Member, IEEE*, and Payam Heydari<sup>®</sup>, *Fellow, IEEE* 

Abstract—Multi-channel biosignal recording systems that employ a shared-reference scheme and achieve high common-mode rejection ratio (i.e., CMRR > 80dB) have been reported in recent works. While it is well-understood that a shared-reference scheme causes impedance mismatch at the input terminals of bioamplifier, and thus limits the maximum achievable CMRR, a theoretical study that can provide quantitative assessment of this source of degradation is still lacking. This brief provides an equivalent electrical circuit model of the input interface consisting of an electrode array and bioamplifiers, followed by a complete analysis to formulate the CMRR degradation. Simulation results based on a previously designed and fabricated 32-channel neural recording front-end in a 180nm CMOS process are presented, exhibiting close agreement with the theory.

Index Terms—Common mode rejection ratio, multi-channel, biosignal acquisition, shared reference, impedance mismatch, CMRR degradation.

## I. INTRODUCTION

THE PRESENCE of common-mode interference (CMI) is highly undesirable in biomedical signal acquisition and processing, as it necessitates an excessive dynamic range, higher linearity and additional high-Q notch filtering, without which the system will completely fail to operate. Historically, the 50/60-Hz power-line interference observed in biopotential recordings (e.g., two/three electrode ECG monitoring) has been thoroughly studied in a number of prior works [1]–[3], which provide detailed analysis and different mitigation techniques. More recently, with the advent of miniaturized electrode arrays and nanoscale electronics, implantable biomedical devices have introduced a new source of interference, namely the stimulation artifacts in bi-directional brain-machine interfaces. Similar to the power-line interference, electrical

Manuscript received May 21, 2020; revised July 5, 2020; accepted July 15, 2020. Date of publication July 22, 2020; date of current version December 21, 2020. This brief was recommended by Associate Editor J. Goes. (Corresponding author: Omid Malekzadeh-Arasteh.)

Omid Malekzadeh-Arasteh, Ahmad Reza Danesh, and Payam Heydari are with the Department of Electrical Engineering and Computer Science, University of California, Irvine, CA 92697 USA (e-mail: omalekza@uci.edu; ahmadred@uci.edu; payam@uci.edu).

An H. Do is with the Department of Neurology, University of California at Irvine, Irvine, CA 92697 USA (e-mail: and@uci.edu).

Zoran Nenadic is with the Department of Biomedical Engineering, University of California at Irvine, Irvine, CA 92697 USA (e-mail: znenadic@uci.edu).

Color versions of one or more of the figures in this article are available online at https://ieeexplore.ieee.org.

Digital Object Identifier 10.1109/TCSII.2020.3011180

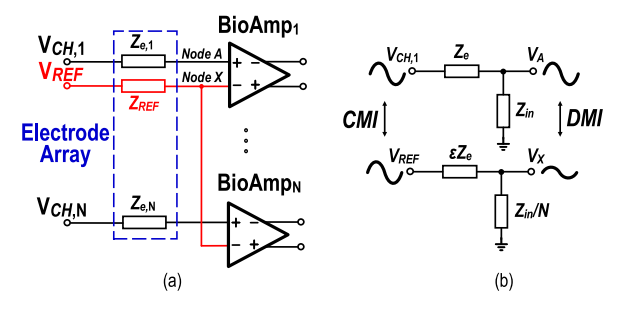


Fig. 1. (a) Conventional *N*-channel biosignal acquisition front-end with shared reference (b) Simplified electrical model of the input interface [4].

stimulation produces an in-band blocker with large common-mode component (>100mV) that is orders of magnitude greater than the biosignal (10-100 $\mu$ V).

While existing architectures rely on active shielding and bioamplifiers with high common-mode rejection ratio (CMRR) to suppress CMI, there still remains a major bottleneck within multi-channel recording systems that employ a sharedreference scheme. Shown in Fig. 1(a), a typical N-channel biosignal acquisition front-end consists of an electrode array and a set of differential bioamplifiers (BioAmps). Each BioAmp is connected to a biosignal electrode, as indicated by Node A for every channel, and a shared reference electrode, Node X. Since the latter node is attached to all N number of BioAmps, a systematic impedance imbalance exists, which together with the electrode's mismatch, give rise to unequal potential divider effect [1]. This phenomenon converts CMI present at the tissue-electrode interface to differential-mode interference (DMI), thereby limiting the maximum achievable CMRR in the system.

A simplified electrical model of the input interface for an N-channel neural amplifier system was presented in [4]. This model assumes an electrode impedance of  $Z_e$  and an input impedance of  $Z_{in}$  for each BioAmp, as depicted in Fig. 1(b). Hence, the total CMRR ( $CMRR_T$ ) is expressed, as follows [4]:

$$\frac{1}{CMRR_T} = \frac{1}{ICMRR} + \frac{2(N\epsilon - 1)}{2|Z_{in}/Z_e| + N\epsilon + 1}$$
(1)

where ICMRR and  $\epsilon$  represent the intrinsic CMRR of bioamplifier and the mismatch factor for the shared reference electrode, respectively. The second term in Eq. (1) approximates the CMRR degradation due to the unbalanced voltage

1549-7747 © 2020 IEEE. Personal use is permitted, but republication/redistribution requires IEEE permission. See https://www.ieee.org/publications/rights/index.html for more information.

152

division at the electrode-BioAmp interface. However, in deriving (1), a number of limiting assumptions have been adopted, which must be revised. For instance, 1) The input impedance of BioAmp is a combination of differential and common-mode impedances, thus  $Z_{in}$  needs to be revised in the foregoing analysis to account for both contributions. 2) When speaking of CMI to DMI conversion, it is important to note that the AC current flowing through the reference electrode may not be equally distributed among all BioAmps, as will be discussed later. Thus,  $Z_{in}/N$  illustrated in Fig. 1(b) needs to be modified, accordingly. This brief provides a complete electrical circuit model of the input interface, followed by a generalized theory of CMRR degradation in multi-channel bioamplifiers.

## II. PROPOSED INPUT INTERFACE MODEL

In this section, the conventional *N*-channel biosignal acquisition front-end in Fig. 1(a) is revisited, where a complete representation of the input impedance of BioAmp is provided. Next, an equivalent electrical circuit model of the input interface is developed that lays the foundation for the subsequent analysis.

## A. BioAmp Input Impedance

A widely used BioAmp is the capacitvely-coupled operational transconductance amplifier (OTA) that uses pseudoresistors in the feedback network [5], as depicted in Fig. 2(a). Considering that the input impedance of BioAmp can be expressed in terms of a differential-mode ( $Z_{DM}$ ) and a common-mode ( $Z_{CM}$ ) component, a simple T-network is used to illustrate the input impedance of BioAmp, as shown in Fig. 2(b). Since OTA typically employs a cascade of two stages, it is modeled by a differential input pair with an effective transconductance of  $A \times g_m$ . To derive  $Z_{DM}$ , OTA is placed in a feedback configuration similar to BioAmp with both common loads ( $Z_{L,1}$ ) and differential-mode loads ( $Z_{L,2}$ ) present at the output, as shown in Fig. 2(c). Using half-circuit model, the odd impedance ( $Z_{odd}$ ) representing half of  $Z_{DM}$  is readily calculated, as follows:

$$Z_{odd} = Z_1 + \frac{(r_{o,p} \| r_{o,n}) \| (Z_{L,1} \| \frac{Z_{L,2}}{2}) + Z_2}{1 + Ag_m \left[ (r_{o,p} \| r_{o,n}) \| (Z_{L,1} \| \frac{Z_{L,2}}{2}) \right]} \approx Z_1 \quad (2)$$

where  $r_{o,p}$  and  $r_{o,n}$  denote the output resistance of PMOS and NMOS transistors, respectively. Similarly,  $Z_{CM}$  is found by taking into account the source degeneration and disregarding  $Z_{L,2}$ , as depicted in Fig. 2(d). Using half-circuit model, the even impedance ( $Z_{even}$ ), which is twice as large as  $Z_{CM}$ , is readily calculated:

$$Z_{even} = Z_1 + Z_p ||[Z_2 + (Z_{L,1}||r_{o,p})] \approx Z_1 + Z_2$$
 (3)

where  $Z_p$  denotes the impedance of the parasitic capacitance at each input terminal of OTA. For a typical closed-loop gain of 40 dB, BioAmp requires a capacitive ratio of  $C_1/C_2=100$ . Therefore,  $Z_{CM}$  of BioAmp is mostly dominated by the equivalent impedance of the feedback capacitor ( $C_2$ ) and the parallel parasitic capacitance, which is approximated by  $Z_2$ .

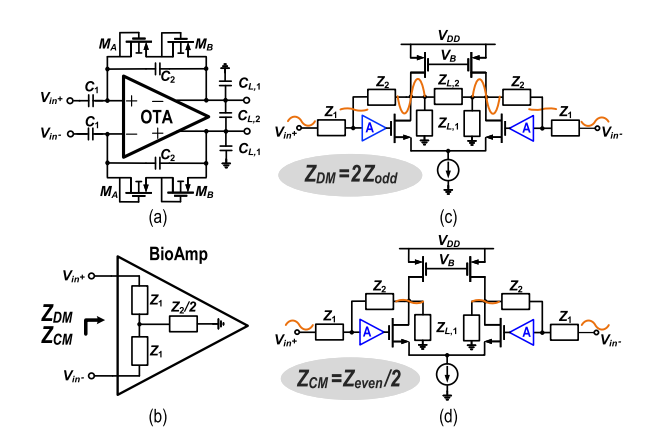


Fig. 2. BioAmp (a) topology (b) input impedance model (c) differential-mode and (d) common-mode input impedance.

# B. Electrode-BioAmp Interface

IEEE TRANSACTIONS ON CIRCUITS AND SYSTEMS—II: EXPRESS BRIEFS, VOL. 68, NO. 1, JANUARY 2021

Based on the impedance representation in Fig. 2(b), the input impedance of each BioAmp is modeled using a two-port network, and thus an equivalent electrical circuit model for the electrode-BioAmp interface is developed, as depicted in Fig. 3. For each channel,  $Z_{in^+}$  represents the input impedance seen from the channel electrode accounting for the loading effects of the reference electrode and the remaining BioAmps. Likewise,  $Z_{in^-}$  represents the input impedance seen from the reference electrode including the loading effect of channel electrode. By further inspecting the input interface, two observations are made regarding the CMRR degradation.

Unlike the circuit shown in Fig. 1(b), the two-port network representation exhibits a "coupled path" between nodes A and X [6]. Hence, in the absence of the shared connections at node X, the maximum achievable CMRR for a single channel is mainly determined by impedance mismatch between the channel and reference electrodes relative to  $Z_{CM}$ . Meanwhile, the shared connection in N-channel configuration creates unequal loading on each side of the two-port network, which becomes a major source of CMI to DMI conversion. While it is intuitive that the loading effect is more significant on the shared node, the extent of CMRR degradation heavily depends on how CMI appears across the channels with respect to the shared reference electrode, as will be discussed in Section III-B. It is noteworthy that several prior works have employed positive feedback techniques (e.g., capacitive neutralization) to significantly boost  $Z_{DM}$  as a way to circumvent the loading effect. However, these techniques are known to pose instability issues, lower  $Z_{CM}$ , and degrade the maximum achievable CMRR, as mentioned above.

### III. THEORETICAL ANALYSIS

## A. Total and Intrinsic CMRR Derivations

Similar to Eq. (1), it is possible to define an overall CMRR for a multi-stage differential system in terms of the following transfer functions: differential-to-differential mode gain  $(G_{DD})$ , common-to-common mode gain  $(G_{CC})$ , common-to-differential mode gain  $(G_{DC})$  and differential-to-common mode gain  $(G_{CD})$ . Following the analysis in [6] and assuming negligible contributions of  $G_{CD}$  product terms, the total

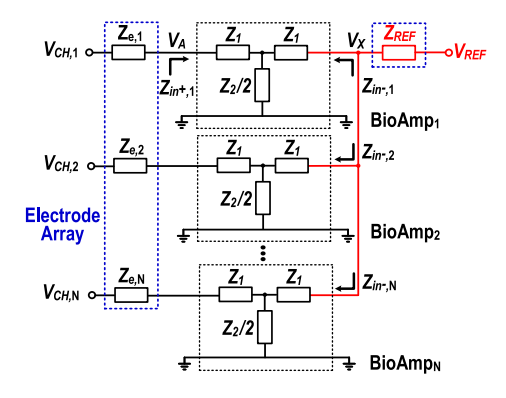


Fig. 3. Proposed input interface model.

CMRR for n differential stages in cascade is

$$CMRR_T^{-1} \approx \sum_{k=1}^{n} (CMRR_k)^{-1}, \tag{4}$$

$$CMRR_{k} = \begin{cases} \left(\frac{G_{DD}}{G_{DC}}\right)_{1}, & \text{for } k = 1\\ \left(\frac{G_{DD}}{G_{DC}}\right)_{k} \prod_{i=1}^{k-1} \left(\frac{G_{DD}}{G_{CC}}\right)_{i}, & \text{for } k > 1 \end{cases}$$
(5)

In a typical biosignal recording system, the first stage consists of the electrode-BioAmp interface, followed by a number of subsequent amplification stages. While it is straightforward to achieve high  $G_{DD}/G_{CC}$  ratio for each gain stage by employing a fully differential architecture, it becomes challenging to improve  $G_{DD}/G_{DC}$  which is mostly limited by the mismatches associated with on-chip passive and active devices. Since  $G_{DD}/G_{CC}$  ratio for each differential amplification stage is very large,  $(G_{DD}/G_{DC})_{n=2}$  has dominant effect on the total CMRR. To quantify the main contributing sources to  $(G_{DD}/G_{DC})_{n=2}$  (i.e., ICMRR), mismatches are considered for the BioAmp model of Figs. 2(c)-(d) and the ICMRR is readily calculated, as follows [7]:

$$\frac{1}{ICMRR} \approx \frac{1}{CMRR_{OTA}} + \frac{1}{CMRR_{FB}}$$

$$\approx \frac{\Delta g_{m,A}}{g_{m,A}(1 + 2g_{m,A}Z_{SS})} + \frac{\frac{\Delta Z_1}{Z_1} - \frac{\Delta Z_2}{Z_2}}{1 - \frac{\Delta Z_1}{Z_{Z_1}} + \frac{\Delta Z_2}{Z_{Z_2}}} \tag{6}$$

where  $[g_{m,A}, \Delta g_{m,A}]$ ,  $[Z_1, \Delta Z_1]$ ,  $[Z_2, \Delta Z_2]$  and  $Z_{SS}$  represent the mean-value transconductance of OTA's first stage and its mismatch, feedback elements impedance and their associated mismatches and source degeneration impedance, respectively. As seen in Eq. (6), the ICMRR is limited by transconductance and feedback impedance mismatches. To minimize the contribution of the former,  $Z_{SS}$  can be increased. Meanwhile, the latter term is heavily dependent on the technology node and layout techniques (e.g., minimum unit capacitance, commoncentroid placement) which sets an upper-limit for ICMRR if no trimming or enhancement technique is employed.

# B. Input Interface CMRR Derivation

The electrode-BioAmp interface is yet another determining factor that affects the overall CMRR, as it constitutes the first stage of differential acquisition without any amplification. To avoid CMRR degradation, it is imperative to

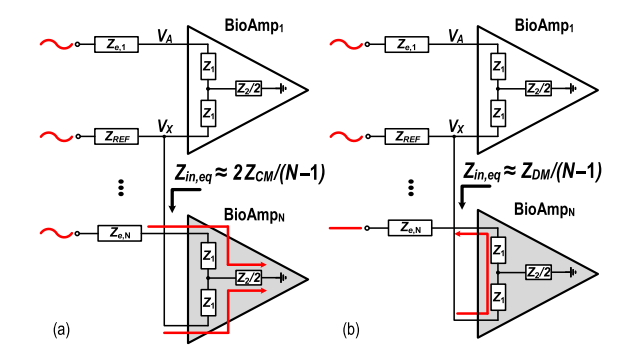


Fig. 4. Electrode-BioAmp interface with (a) CMI across all channels (b) CMI across a single channel.

minimize  $(G_{DD}/G_{DC})_{n=1}$  which is mainly determined by the impedance imbalance in the interface. In this brief, the extent of impedance imbalance between nodes A and X for a given channel (BioAmp<sub>1</sub> in Figs. 4(a)-(b)) is studied for two general case scenarios of CMI. Starting with Fig. 4(a), CMI is assumed to be uniformly present across all channels with respect to the reference electrode. The common-mode AC currents passing through the channel and reference electrodes are absorbed by  $Z_{CM}$  of each BioAmp. Thus, it can be mathematically shown that the shared node experiences less loading effect as the equivalent input impedance looking into all remaining BioAmps is  $\approx 2Z_{CM}/(N-1)$ , which is much larger than  $Z_{REF}$ . On the other hand, if only one channel experiences CMI with respect to the reference electrode (BioAmp<sub>1</sub> in Fig. 4(b)), the equivalent input impedance at the shared node looking into all remaining BioAmps is significantly reduced, giving rise to severe loading effect. Depicted in Fig. 4(b), the AC current flowing from the reference electrode into the interference-free BioAmps circulates back through the channel electrodes provided that  $(Z_{e,j}+Z_1) \ll Z_2$  for  $j=1,\ldots,N$ , which holds true for a typical BioAmp. Hence, the equivalent input impedance looking into BioAmps reduces to  $\approx Z_{DM}/(N-1)$ , causing significant CMRR degradation.

Since loading on the shared node depends on the number of channels experiencing CMI with respect to the reference electrode, it becomes a necessity to obtain the input interface CMRR,  $(G_{DD}/G_{DC})_{n=1}$ , for a given channel (e.g., BioAmp<sub>1</sub>) in terms of the voltage transfer functions (TFs) from all inputs to node A and X. For this reason, five distinct voltage TFs are identified in the input interface: (I)  $V_A/V_{CH,1}$ , (II)  $V_A/V_{CH,m}$  where  $m=2,\ldots,N$ , (III)  $V_A/V_{REF}$ , (IV)  $V_X/V_{REF}$  and (V)  $V_X/V_{CH,j}$  where  $j=1,\ldots,N$ . Shown in Fig. 5(a), each TF is distinguished by its signal path marked with an arrow. In addition, the channel electrode and T-network impedances are substituted by a  $\pi$ -equivalent circuit, as seen in the dotted boxes. It is worth noting that contributions from TF-II is negligible and therefore, is not considered in the derivations for the sake of brevity.

To find an expression for TF-I, -III and -IV,  $Z_{in^+,1}$  and  $Z_{in^-,j}$  for  $j=1,\ldots,N$  should be derived. To begin with, Z-parameters of the two-port network modeling the BioAmp are calculated, as follows:

$$Z_{param} = \begin{bmatrix} Z_1 + Z_2/2 & Z_2/2 \\ Z_2/2 & Z_1 + Z_2/2 \end{bmatrix}$$
 (7)

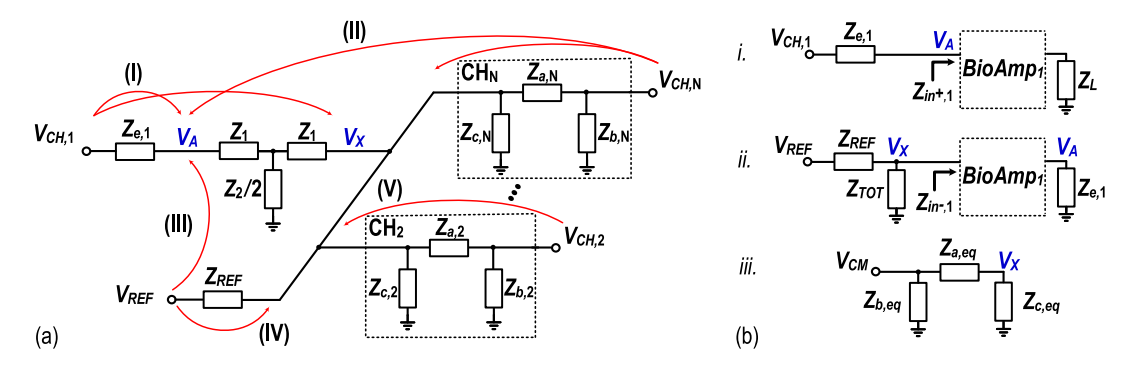


Fig. 5. (a) Signal paths in the input interface considered for voltage transfer function analysis (b) equivalent circuits.

Subsequently,  $Z_{in^+,1}$  terminated by  $Z_L$  is determined:

$$Z_{in^+,1} \triangleq Z_{11} - \frac{Z_{12}Z_{21}}{Z_{22} + Z_L} = (Z_1 + Z_L) \| (Z_2/2) + Z_1$$
 (8)

where

$$Z_L^{-1} = Z_{TOT}^{-1} + Z_{REF}^{-1} (9)$$

and

$$Z_{TOT}^{-1} = \sum_{i=2}^{N} (Z_{in^-,i})^{-1}$$
 (10)

Similarly,  $Z_{in^-,j}$  terminated by the channel electrode,  $Z_{e,j}$  for  $j = 1, \dots, N$ , is calculated to be:

$$Z_{in^-,j} \triangleq Z_{22} - \frac{Z_{21}Z_{12}}{Z_{11} + Z_{e,j}} = (Z_1 + Z_{e,j}) \| (Z_2/2) + Z_1$$
 (11)

By examining the equivalent circuit of Fig. 5(b)(i), TF-I is derived in terms of  $Z_{in^+,1}$  and  $Z_L$ , expressed in Eqs. (8) and (9):

$$\frac{V_A}{V_{CH,1}} = \frac{1}{1 + Z_{e,1}/Z_{in^+,1}} \tag{12}$$

Similarly, TF-III and TF-IV are calculated based on the equivalent circuit of Fig. 5(b)(ii), i.e.,

$$\frac{V_A}{V_{REF}} \approx \frac{Z_{e,1}/Z_{REF}}{1 + Z_{in^-,1}/Z_L}$$
 (13)

$$\frac{V_A}{V_{REF}} \approx \frac{Z_{e,1}/Z_{REF}}{1 + Z_{in^-,1}/Z_L}$$

$$\frac{V_X}{V_{REF}} = \frac{1}{1 + Z_{REF} \sum_{i=1}^{N} Z_{in^-,i}^{-1}}$$
(13)

In deriving Eq. (13), it is assumed  $Z_2 \gg Z_1 + Z_{e,1}$ , which holds true for a typical BioAmp.

The  $\pi$ -equivalent circuit for each channel, as depicted in Fig. 5(a), helps simplify the calculations involving the effect of TF-V. By applying Y- $\Delta$  transformation, each impedance in  $\pi$ -network is readily expressed for the *j*-th channel, as follows:

$$Z_{a,j} = Z_{e,j} + 2Z_1 + \frac{2(Z_{e,j} + Z_1)(Z_1)}{Z_2}$$
 (15)

$$Z_{b,j} = Z_{e,j} + Z_1 + Z_2(1 + \frac{Z_{e,j}}{2Z_1})$$
 (16)

$$Z_{c,j} = Z_1 + \frac{Z_2}{2} \left(1 + \frac{1}{1 + \frac{Z_{e,j}}{Z_1}}\right) \tag{17}$$

Assuming that CMI appears across the reference and Mnumber of channels, the equivalent circuit of Fig. 5(b)(iii) is obtained by merging parallel  $\pi$ -networks with  $Z_{REF}$ , whose equivalent impedances are derived, as follows:

$$Z_{a,eq}^{-1} = \sum_{i=1}^{M} (Z_{a,i})^{-1} + Z_{REF}^{-1}$$
 (18)

$$Z_{b,eq}^{-1} = \sum_{i=1}^{M} (Z_{b,i})^{-1}$$
(19)

$$Z_{c,eq}^{-1} = \sum_{i=1}^{M} Z_{c,i}^{-1} + \sum_{i=M+1}^{N} Z_{in^{-},i}^{-1}$$
 (20)

Hence, the total voltage contribution to node X (i.e., summation of TF-IV and TF-V) is readily calculated:

$$\frac{V_X}{V_{CM}} = \frac{Z_{c,eq}}{Z_{a,eq} + Z_{c,eq}},$$
(21)

Based on Eqs. (12), (13) and (14), the input interface differential-to-differential mode gain  $(G_{DD,int})$  is defined:

$$G_{DD,int} \triangleq (V_A - V_X)/V_{DM}$$

$$= \left(\frac{V_A}{V_{CH,1}} - \frac{V_A}{V_{REF}} + \frac{V_X}{V_{REF}}\right)\Big|_{V_{CH,1} = V_{REF} = V_{DM}}$$
(22)

The voltage contribution of  $(V_X/V_{CH,1})|_{V_{CH,1}=V_{DM}}$  is omitted from the above expression since it has negligible effect. Similarly, based on Eqs. (12), (13) and (21), the input interface common-to-differential mode gain  $(G_{DC,int})$  is defined:

$$G_{DC,int} \triangleq (V_A - V_X)/V_{CM}$$

$$= \left(\frac{V_A}{V_{CH,1}} + \frac{V_A}{V_{REF}}\right)\Big|_{V_{CH,1} = V_{REF} = V_{CM}} - \frac{V_X}{V_{CM}} \quad (23)$$

Finally, the total and the input interface CMRR, assuming  $(Z_2 \gg Z_1 \gg Z_{REF}, Z_{e,j} \text{ for } j = 1, ..., N)$ , are derived:

$$\frac{1}{CMRR_T} = \frac{1}{ICMRR} + \frac{1}{CMRR_{int}}$$
 (24)

$$CMRR_{int} = \left(\frac{G_{DD}}{G_{DC}}\right)_{int} = \frac{1 + \frac{1}{1 + \frac{Z_{REF}}{2Z_{1}} \times N}}{1 - \frac{1}{1 + \frac{Z_{REF}}{\frac{Z_{2}}{M} \left\|\frac{Z_{2}}{N-M}}}}$$
(25)

where ICMRR is previously defined in Eq. (6). The closedform expression in Eq. (25) shows that for an N-channel acquisition front-end, the maximum CMRR is achieved when M=N and degrades with higher values of N.

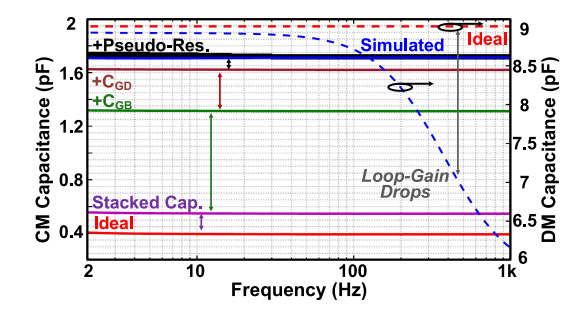


Fig. 6. CM and DM capacitance seen from the input terminals of BioAmp (red and blue traces depict the ideal and simulated results, respectively).

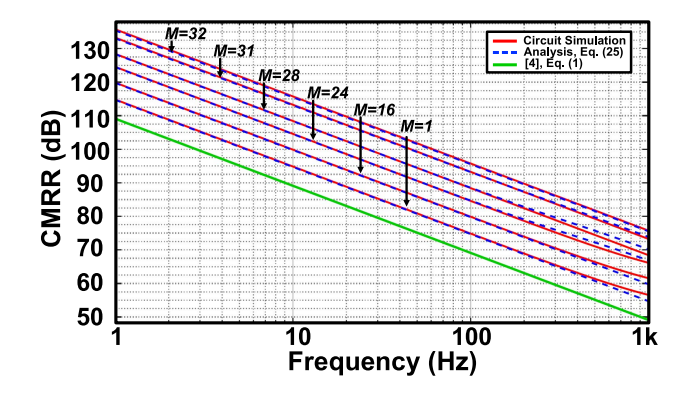


Fig. 7. Simulated and predicted CMRR<sub>int</sub> given *M*-number of channels experiencing CMI in a 32-channel neural recording system.

#### IV. NUMERICAL RESULTS

In this section, theoretical and circuit simulation results for a previously designed and fabricated 32-channel neural recording system in a 180nm CMOS process [8] are presented.

# A. BioAmp CM & DM Input Capacitance

Simulated input capacitance of the BioAmp in [8] are compared with the model of Section II-A. Each input and feedback capacitor is realized using MIM stacked structure with a capacitance of 18 and 0.2 pF, respectively. Common-mode (CM) and differential-mode (DM) capacitance for the BioAmp are shown in Fig. 6. Given that CM capacitance deviates from the ideal value of 0.4 pF, a behavioral model is used for deembedding the parasitic capacitances which contribute  $\sim$ 640fF to each input terminal of OTA. Since no chopping mechanism is employed in the BioAmp, the input pair transistors are sized adequately to reduce flicker noise and therefore, introduce significant gate-to-bulk  $(C_{GB})$  and gate-to-drain  $(C_{GD})$  parasitic capacitance. Furthermore, DM capacitance decreases as the loop gain of the BioAmp drops beyond the 3-dB bandwidth which gives rise to higher impedance, as predicted by Eq. (2) and deduced from Fig. 6.

## B. Input Interface CMRR

The simulated input interface CMRR of the fabricated 32-channel electrocorticography (ECoG) acquisition front-end in [8] is compared with Eq. (25) and the second term of Eq. (1). Shown in Fig. 7, the simulated and predicted CMRR<sub>int</sub> versus frequency is plotted for different values of *M*, assuming

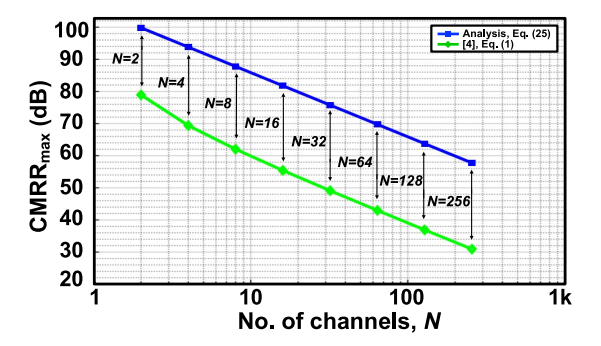


Fig. 8. Maximum achievable CMRR for a multi-channel biosignal acquisition.

an electrode impedance of  $1 \text{ k}\Omega$  (typical for ECoG electrodes). As depicted, the CMRR degradation due to the impedance imbalance increases with fewer number of channels experiencing CMI with respect to the reference electrode, which closely follows the analysis in this brief. Assuming that *ICMRR* and electrode mismatches are not the limiting factors, the maximum achievable CMRR (*CMRR*<sub>max</sub>), coinciding with *M*=*N*, is found by evaluating Eq. (25) and Eq. (1) for different number of channels and the same impedance values (at 1 kHz) used in Section IV-A, as shown in Fig. 8.

## V. CONCLUSION

In this brief, a detailed analysis of CMRR degradation is presented based on a proposed electrical circuit model of the input interface for a multi-channel biosingal recording system, exhibiting close agreement with circuit simulations.

## ACKNOWLEDGMENT

The authors would like to thank Haoran Pu for helpful technical discussions.

## REFERENCES

- J. C. Huhta and J. G. Webster, "60-Hz interference in electrocardiography," *IEEE Trans. Biomed. Eng.*, vol. BME-20, no. 2, pp. 91–101, Mar 1973
- [2] B. B. Winter and J. G. Webster, "Reduction of interference due to common mode voltage in biopotential amplifiers," *IEEE Trans. Biomed. Eng.*, vol. BME-30, no. 1, pp. 58–62, Jan. 1983.
- [3] R. Pallas-Areny, "Interference-rejection characteristics of biopotential amplifiers: A comparative analysis," *IEEE Trans. Biomed. Eng.*, vol. 35, no. 11, pp. 953–959, Nov. 1988.
- [4] K. A. Ng and Y. P. Xu, "A low-power, high CMRR neural amplifier system employing CMOS inverter-based OTAs with CMFB through supply rails," *IEEE J. Solid-State Circuits*, vol. 51, no. 3, pp. 724–737, Mar. 2016.
- [5] R. R. Harrison and C. Charles, "A low-power low-noise CMOS amplifier for neural recording applications," *IEEE J. Solid-State Circuits*, vol. 38, no. 6, pp. 958–965, Jun. 2003.
- [6] R. Pallás-Areny and J. G. Webster, "Common mode rejection ratio for cascaded differential amplifier stages," *IEEE Trans. Instrum. Meas.*, vol. 40, no. 4, pp. 677–681, Aug. 1991.
- [7] R. Pallás-Areny and J. G. Webster, "Common mode rejection ratio in differential amplifiers," *IEEE Trans. Instrum. Meas.*, vol. 40, no. 4, pp. 669–676, Aug. 1991.
- [8] O. Malekzadeh-Arasteh et al., "An energy-efficient CMOS dual-mode array architecture for high-density ECoG-based brain-machine interfaces," IEEE Trans. Biomed. Circuits Syst., vol 14, no. 2, pp. 332–342, Apr. 2020.